The use of detrital mineral cooling ages to evaluate steady state assumptions in active orogens: An example from the central Nepalese Himalaya

K. W. Ruhl and K. V. Hodges

Department of Earth, Atmospheric and Planetary Sciences, Massachusetts Institute of Technology, Cambridge, Massachusetts, USA

Received 14 July 2004; revised 16 February 2005; accepted 11 April 2005; published 23 August 2005.

[1] The distribution of detrital mineral cooling ages in modern sediments has been proposed as a proxy for long-term, catchment-averaged erosion rates in developing orogens. However, the applicability of this potentially valuable tool hinges on restrictive assumptions regarding a catchment's steady state thermal and topographic evolution. In this paper, we outline a method by which these assumptions can be tested through statistical comparisons of cooling age distributions for detrital minerals and the hypsometric curves for their source regions using cumulative synoptic probability density functions. Our approach is illustrated with new detrital muscovite $^{40}Ar/^{39}Ar$ dates from the Marsyandi River valley, in the central Nepalese Himalaya. One of three studied catchments (Nyadi Khola) showed the strong correlation of hypsometry and cooling ages expected for steady state conditions over the 11 to 2.5 Ma time frame. The pattern of mismatch between hypsometry and cooling age distribution in the other catchments suggests that spatially nonuniform and transient erosional processes may be responsible for departure from steady state. Cooling age distribution comparisons for samples collected from nearby localities, samples collected in different years, and different grain size fractions from the same sample were used to evaluate sampling fidelity over a range of spatial scales (200 to 2590 km^2). We found that approximately 50 analyses from a single sediment sample adequately characterize the cooling age signal for tributary catchments with simple erosional histories. However, because of temporally and spatially transient erosion, a specific detrital sample is unlikely to adequately characterize the complex signal in trunk stream sediments that integrate information from several large tributaries.
Citation: Ruhl, K. W., and K. V. Hodges (2005), The use of detrital mineral cooling ages to evaluate steady state assumptions in active orogens: An example from the central Nepalese Himalaya, *Tectonics*, *24*, TC4015, doi:10.1029/2004TC001712.

0278-7407/05/2004TC001712$12.00

1. Introduction

[2] Testing the hypothesis that climate and erosion can exert fundamental controls on orogen-scale tectonics requires the development of reliable techniques for quantifying tectonic and geomorphic process rates at a variety of spatial and temporal scales. Detrital mineral dating techniques for ancient and modern deposits have been applied to a wide range of tectonic and geomorphic problems (see, for example, a review of $^{40}Ar/^{39}Ar$ applications by *Hodges et al.* [2005]). These include, for example, determining sediment source regions, constraining the timing of source region uplift and exhumation, investigating the erosion-transport interval or lag time for orogenic detritus, studying paleodrainage patterns, and investigating modern erosional patterns and sedimentary processes [e.g., *Kelley and Bluck*, 1989; *Brandon and Vance*, 1992; *Clift et al.*, 1996; *Adams and Kelley*, 1998; *Garver et al.*, 1999; *Spiegel et al.*, 2000; *Bullen et al.*, 2001; *Bernet et al.*, 2001, 2004a; *Carrapa et al.*, 2003; *Najman et al.*, 2003].

[3] Recently, thermochronologic study of detrital minerals in modern stream sediments has been proposed as an efficient means of estimating long-term, catchment-wide erosion rates [*Brewer et al.*, 2003]. However, these estimates are strongly dependent on a series of assumptions regarding the topographic evolution of a specific river catchment. Here we present a straightforward method for testing several of these assumptions, and thus for judging the suitability of a particular data set for erosion rate modeling. More importantly, we show how detrital mineral thermochronology can be used to evaluate the most fundamental assumption of all: that the topography of a drainage system and the thermal structure beneath it have remained unchanged (i.e., at "steady state") at appropriate times throughout the erosional period. Our approach is illustrated using a new data set from the Marsyandi River system in the central Nepalese Himalaya, the site of previous reconnaissance studies conducted by *Brewer et al.* [2003, 2005].

2. Detrital Mineral Thermochronology and Erosion Rates

[4] As suggested by *Brewer et al.* [2003], the frequency distribution of detrital mineral cooling ages from a modern catchment can be used as a proxy for erosion rate if several assumptions, described in detail below, hold true. Specifically, the range of sampled ages should be proportional to

the elapsed time needed to erode the total relief of the source region, such that a narrower age range indicates a relatively higher erosion rate [*Stock and Montgomery*, 1996; *Brewer et al.*, 2003]. In the one-dimensional case where we ignore the effects of lateral rock advection, a nominal erosion rate (E) over the time period represented by the sampled ages (t_{range}) can be calculated by simply dividing the total elevation range in the catchment (R) by the cooling age range:

$$E = \frac{R}{t_{\text{range}}} \tag{1}$$

Although the range in cooling ages depends only on catchment relief and the erosion rate, the actual ages obtained also depend on the thermal structure of the underlying lithosphere.

[5] A detrital sample's cooling age "signal" can be described in terms of a synoptic probability density function (SPDF). For each crystal that is dated by the $^{40}Ar/^{39}Ar$ method, the calculated age t_m and the analytical uncertainty in that age, as expressed by the standard deviation σ_{t_m}, define a probability density function (PDF) of age (t). Assuming a normal distribution of error:

$$\text{PDF} = \frac{1}{\sigma_{t_m}\sqrt{2\pi}} \exp\left[-\frac{1}{2}\left(\frac{t - t_m}{\sigma_{t_m}}\right)^2\right] \tag{2a}$$

The SPDF for a sample comprising n grains is defined as the sum of the PDFs for each mineral grain dated, with the area under the curve normalized to one:

$$\text{SPDF} = \frac{1}{n}\sum_{i=1}^{n} \text{PDF}(i) \tag{2b}$$

Equation (1) implies that if bedrock is eroded in proportion to surface area, and if the resulting sediment reflects that proportion with high fidelity, the shape of the SPDF should mimic the shape of the hypsometric curve.

[6] In the one-dimensional, forward modeling approach of *Brewer et al.* [2003], steady state catchment hypsometry, topography, and thermal properties are used to define a model cooling age SPDF for a particular long-term average erosion rate experienced by each point in the source catchment. Cooling ages in the catchment are modeled by combining assumed vertical particle trajectories with estimates of the closure isotherm depth as a function of erosion rate and relief. The cooling age (t_c) of a point in the landscape can be calculated from

$$t_c = \frac{(z_x - z_c)}{E} \tag{3}$$

where z_x is the elevation of the sample location, and z_c is the elevation of the closure isotherm. The difference in elevation between valleys and ridges results in longer exhumation paths from z_c to points on the surface on ridges than to points in valleys, such that modeled cooling ages in a catchment increase linearly with elevation. A catchment's hypsometry can be combined with the cooling age–sample elevation relationship (equation (3)) to produce a model SPDF for the catchment (Figure 1b). As erosion rate increases, predicted cooling ages both on ridges and in valleys become younger, and the total range of ages in the catchment becomes narrower [*Brewer et al.*, 2003]. We note that the approach of I. D. Brewer and coworkers could be simplified by constraining the youngest predicted cooling age in the model SPDF to a measured valley bottom bedrock cooling age instead of using an ad hoc thermal model to predict closure isotherm depth (Figure 1b). While *Brewer et al.* [2003] match the position of major peaks in the synthetic SPDF curves with SPDF curves for actual thermochronologic data to estimate a best fit erosion rate, an alternative method is to simply estimate the erosion rate from the catchment relief and width of the cooling age distribution (equation (1)). This alternative approach is the focus of this paper.

[7] Regardless of whether the original *Brewer et al.* [2003] method or our alternative method is used, many of the same a priori assumptions are necessary. In the following paragraphs, we explore these assumptions in greater detail, and examine how some might be tested through comparative studies of detrital mineral cooling age SPDFs and the hypsometric curves for their source regions.

2.1. Assumption 1: Thermal and Topographic Steady States During Exhumation

[8] A variety of steady states have been assumed in tectonic geomorphology studies of active orogens [*Willett and Brandon*, 2002]. The two that are critical for our purposes are time-invariant thermal structure and topography. For either the *Brewer et al.* [2003] method or our method to yield geologically meaningful results, the catchment must have achieved thermal and topographic steady states, and these conditions must have been maintained at appropriate times during the erosional history of the catchment. (We define thermal steady state as implying that the subsurface thermal structure does not change significantly as a function of time. Similarly, we define topographic steady state as the condition for which the hypsometry, or the frequency distribution of surface elevation, of a catchment does not change significantly as a function of time.) For thermochronometers sensitive to closure isotherms that are not significantly perturbed by topography, the "appropriate" time frame is the range of cooling ages determined for minerals in the detrital sample. Thermal and topographic steady states are not independent. Topographic steady state is necessary at long wavelengths (generally >20 km) and over million year timescales in order to maintain thermal steady state because topography defines the surface boundary condition for the thermal structure beneath the landscape [*Mancktelow and Grasemann*, 1997; *Stüwe et al.*, 1994]. Although the temperature field is relatively insensitive to short-term, short-wavelength topographic perturbations, predicted detrital mineral cooling ages are not. As a consequence, a close topologic match between a cooling age SPDF for a sediment sample and the hyposometric curve for

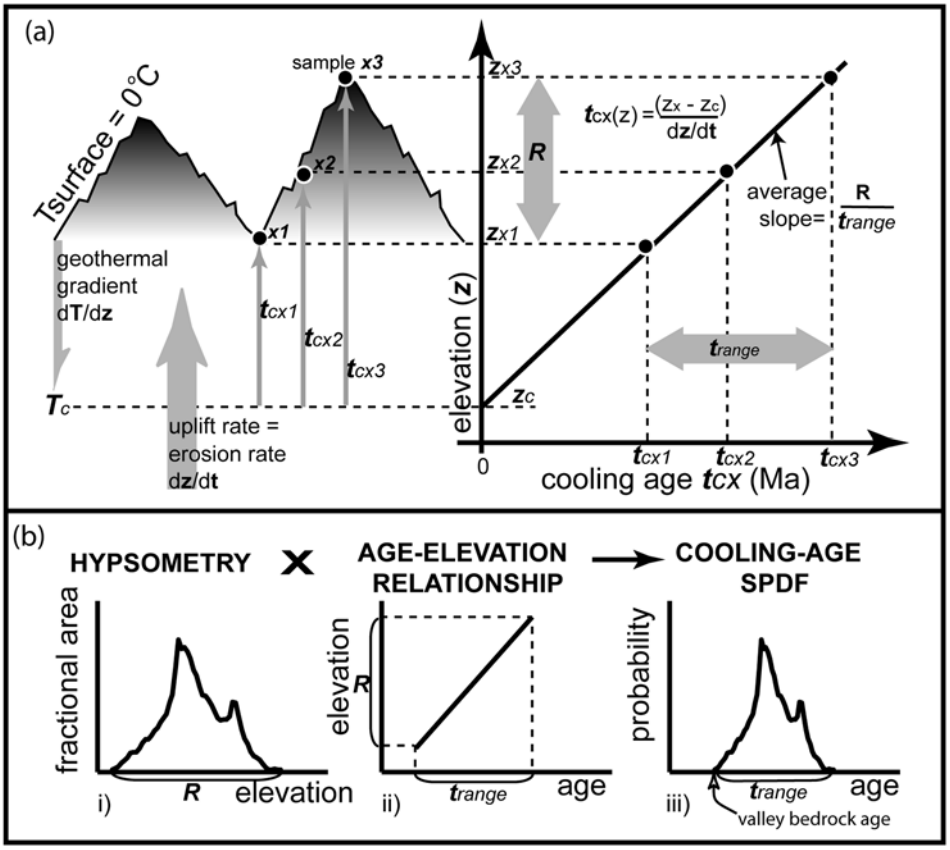

Figure 1. Construction of forward modeled cooling age distribution for a catchment (modified with permission from *Brewer et al.* [2003] and Blackwell Publishing). (a) Cooling age $t_{cx}(z)$ for a sample x at elevation z calculated from the depth z_c of the closure temperature isotherm T_c and a steady state uplift rate equal to erosion rate (dz/dt) can be calculated using the equation shown. Note older t_{cx} for samples at higher elevations. The t_{range} is the total range of cooling ages sampled in the catchment, and R is the total catchment relief. (b) Cooling age SPDF governed by combination of t_{range} and the distribution of land area with elevation (hypsometry). Theoretical cooling age SPDF may be pinned to a measured valley bottom bedrock cooling age if available.

the catchment from which it was collected can provide important evidence that the catchment might be at both topographic and thermal steady states. If relief was decreasing during erosion, the SPDFs of sediments from the catchment would be biased toward older ages than would have been predicted by steady state assumptions. If relief was increasing, comparatively younger material would dominate the cooling age signal.

2.2. Assumption 2: Uniform Erosion Rates Across the Catchment

[9] Another requirement is that erosion rates are spatially uniform throughout the catchment. Lithology and grain size can vary within a catchment such that certain areas yield sediments with finer grain sizes than others at any given time. This grain size variability may be exploited in order to identify catchments with spatially variable erosion using a single sample. Good agreement between cooling age SPDFs for different grain sizes would be expected for small catchments that integrate areas with restricted lithologic variation and insignificant spatial variation in erosion rate. Preferential erosion of certain areas may be reflected in a mismatch between SPDFs for different grain sizes. Alternatively, a significant mismatch indicates lithologic heterogeneity and/or spatial gradients in uplift/erosion regimes within the catchment. For example, if all fine-grained material crops out at low elevations and all coarse-grained material crops out at high elevations, mismatch between fine-grained and coarse-grained SPDFs would be expected even with uniform erosion across the catchment. In this extreme case, area-elevation data can be collected according to mapped lithologic boundaries to produce individual hypsometric curves for the coarse-grained and fine-grained areas. The hypsometric curve and SPDF for each grain size could be combined to estimate erosion rates for each part of the catchment independently, thus providing a direct test of the uniform erosion assumption. Alternatively, multiple detrital samples could be collected at different elevations within the catchment, such that erosion rates may be modeled for various domains within the catchment for comparison.

The same modeled rate for each subsample would be expected for a uniformly eroding catchment.

2.3. Assumption 3: Representative Sampling of the Bedrock in the Catchment

[10] The comparisons listed above do not address directly the question of how well the population of cooling ages, and therefore the erosion rate, is represented by a given sediment sample. Successful erosion rate studies require the collection of enough data to ensure an adequate representation of the distribution of cooling ages within a sample. Moreover, the sediment itself must contain a hypsometrically weighted distribution of cooling ages from the bedrock within the catchment. This requires not only spatially uniform erosion, but no appreciable lag time between erosion and deposition as well. Whereas such assumptions are impossible to test independently from the assumptions described earlier, a close match between cooling age SPDFs and hypsometric curves strongly suggests that the complete range of bedrock cooling ages is present in the detrital sample. If significant mismatches occur, further sampling strategies may be used to establish which assumption might have been violated.

[11] The simplest explanation for sample-to-sample variations in SPDFs from a single locality is that too few grains have been dated from each sample to represent adequately the complete age variation of grains within the sample and, by extension, the catchment. When such mismatches are observed, the obvious strategy is to date more grains from each sample to see if the match improves. If it does not, the mismatch may be caused by uneven distribution of the target mineral, preferential erosion from point sources, or temporary sediment storage that may modulate the relative contribution of sediment from different parts of a catchment [e.g., *Bernet et al.*, 2004b].

[12] Agreement of nearby sample SPDFs is consistent with insignificant sediment storage or preferential erosion at spatial scales of tens to thousands of meters but yields no information on fluctuations due to sediment storage and point source contributions through time. Long-term variations in the detrital signal could be recognized by comparing SPDFs for fluvial terrace deposits with those from modern sediments. It is possible that sediment storage on short timescales and year-to-year signal variation could also be problematic due to frequent landslides in actively uplifting areas. This sort of short-term variability can be explored by comparing samples collected in different years.

3. Application to the Marsyandi Drainage, Central Nepal

[13] In this section, we illustrate our approach using detrital muscovite $^{40}Ar/^{39}Ar$ data from the Marsyandi Valley. Two detrital data sets were evaluated: one from the reconnaissance study of *Brewer et al.* [2005], and a new, more comprehensive data set published here for the first time. The downstream evolution of cooling ages determined as part of the initial study was interpreted by I. D. Brewer and coworkers to reflect a roughly twofold spatial gradient in erosion rates. Modeled erosion rates based on these data vary significantly between adjacent tributary catchments of the Marsyandi River *Brewer et al.* [2005]. The highest estimated erosion rates of ~2 mm/yr were for catchments draining the topographic front of the Himalaya, and estimated rates decreased northward to ~1 mm/yr in catchments that primarily were underlain by low-grade metamorphic rocks of the Tibetan Sedimentary sequence *Brewer et al.* [2005].

[14] In light of the limited size and regional distribution of the *Brewer* [2001] and *Brewer et al.* [2003, 2005] data set, we elected to augment their data with 610 additional $^{40}Ar/^{39}Ar$ age determinations to provide a higher density of sample locations and, more importantly, a larger number of age determinations for each detrital sediment sample.

3.1. Sampling Strategy and Hypsometric Analysis

[15] In Figure 2, thermochronologic sample locations are plotted on a shaded relief map of the study area digital elevation model (DEM). Samples were collected from the Marsyandi River and three of its tributaries chosen for their distinctive hypsometries: the Nyadi Khola, Dudh Khola, and Nar Khola, with drainage areas of 200, 420, and 940 km^2, respectively (Figures 2b–2e). The hypsometric curves shown in Figure 2 were derived from a 90-m DEM (see *Fielding et al.* [1994] for a description of the data set) using ArcInfo drainage area sampling routines with 100-m elevation bins [e.g., *Brozovic et al.*, 1997; *Brocklehurst and Whipple*, 2004]. Solid black curves in Figure 3 illustrate the hypsometry in terms of normalized elevation versus cumulative area to facilitate comparison with cumulative cooling age SPDFs (see below).

[16] We collected the new set of detrital muscovite data with four goals in mind: (1) to compare cooling age SPDFs with hypsometric curves, (2) to evaluate sampling consistency by comparing SPDFs for different samples collected from a single small area, (3) to explore the variability of results obtained for different detrital grain sizes separated from a single sample, and (4) to determine whether or not sediment storage in the catchments might result in interannual differences in detrital sample cooling age SPDFs by comparing the results for newly collected samples with those for samples collected 5 years earlier by I. D. Brewer and colleagues. In addition, the Marsyandi trunk samples integrate the detrital cooling age signal over a much larger area and a broader range in elevation, permitting us to evaluate our sampling and steady state/uniform erosion assumptions over a range of spatial scales.

3.2. The $^{40}Ar/^{39}Ar$ Analytical Methods

[17] Single muscovite grains were analyzed at the $^{40}Ar/^{39}Ar$ laser microprobe facility at the Massachusetts Institute of Technology [*Hodges*, 1998]. They were concentrated by standard techniques and sieved into a variety of size fractions. Between 50 and 175 individual muscovite grains were hand-picked from each sieved separate, providing a range of grain sizes from 250 to 2000 μm. The grains were washed in distilled water and ethanol prior to irradiation at the McMaster University nuclear reactor in Ontario,

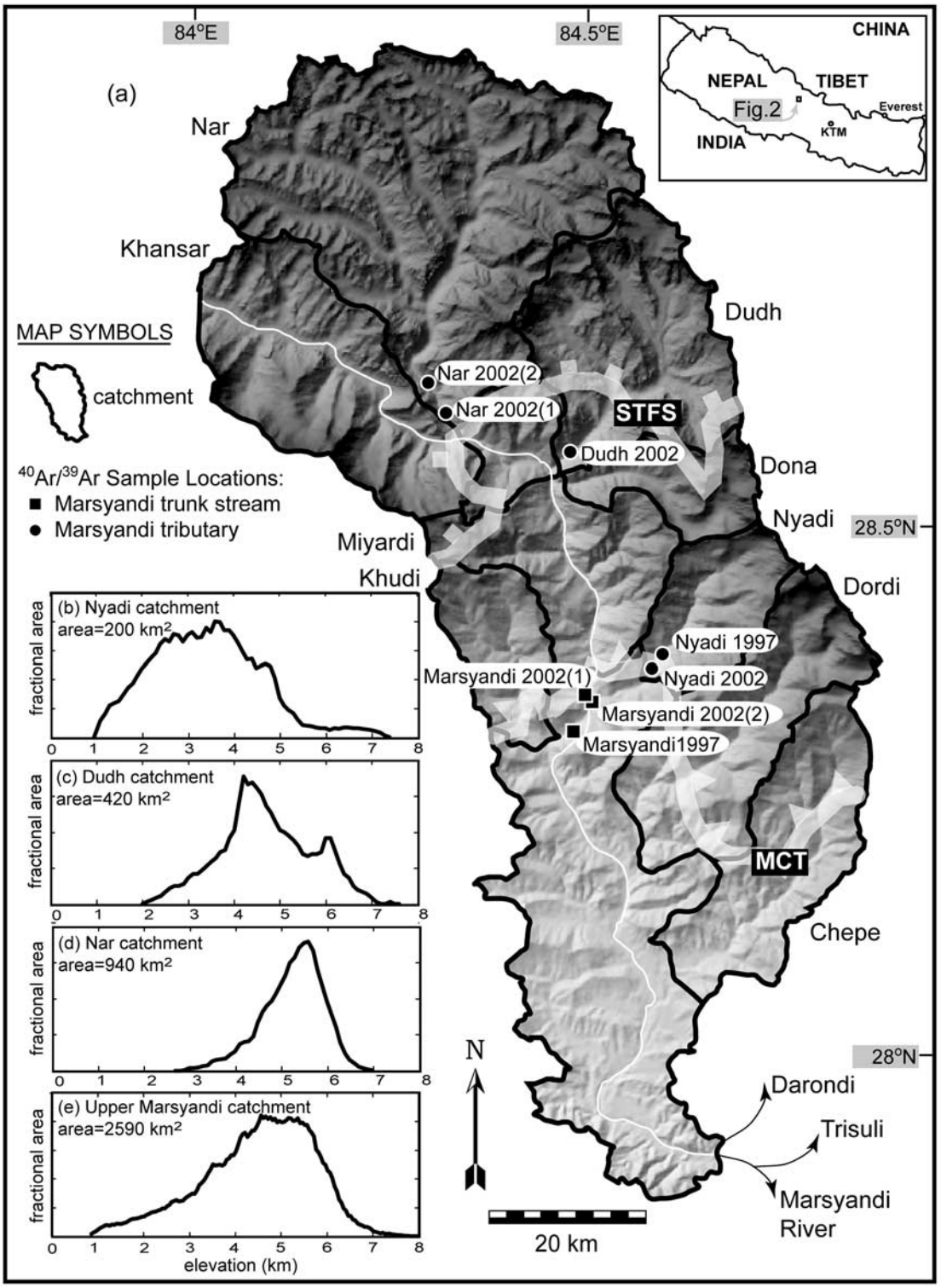

Figure 2. DEM draped over shaded relief map of Marsyandi drainage, detrital sample locations, and hypsometric curves. (a) Marsyandi River drainage with tributary catchments outlined in black, Marsyandi River traced in white, and sample locations marked with solid symbols. Hypsometric curves for (b) Nyadi catchment, (c) Dudh catchment, (d) Nar catchment, and (e) upper Marsyandi catchment drainage area above Marsy1 sample location. Thick white lines indicate approximate trace of a strand of the South Tibetan Fault system (STFS, mentioned in text) and the Main Central Thrust (MCT) zone for reference [after *Colchen et al.*, 1986; *Hodges et al.*, 1996].

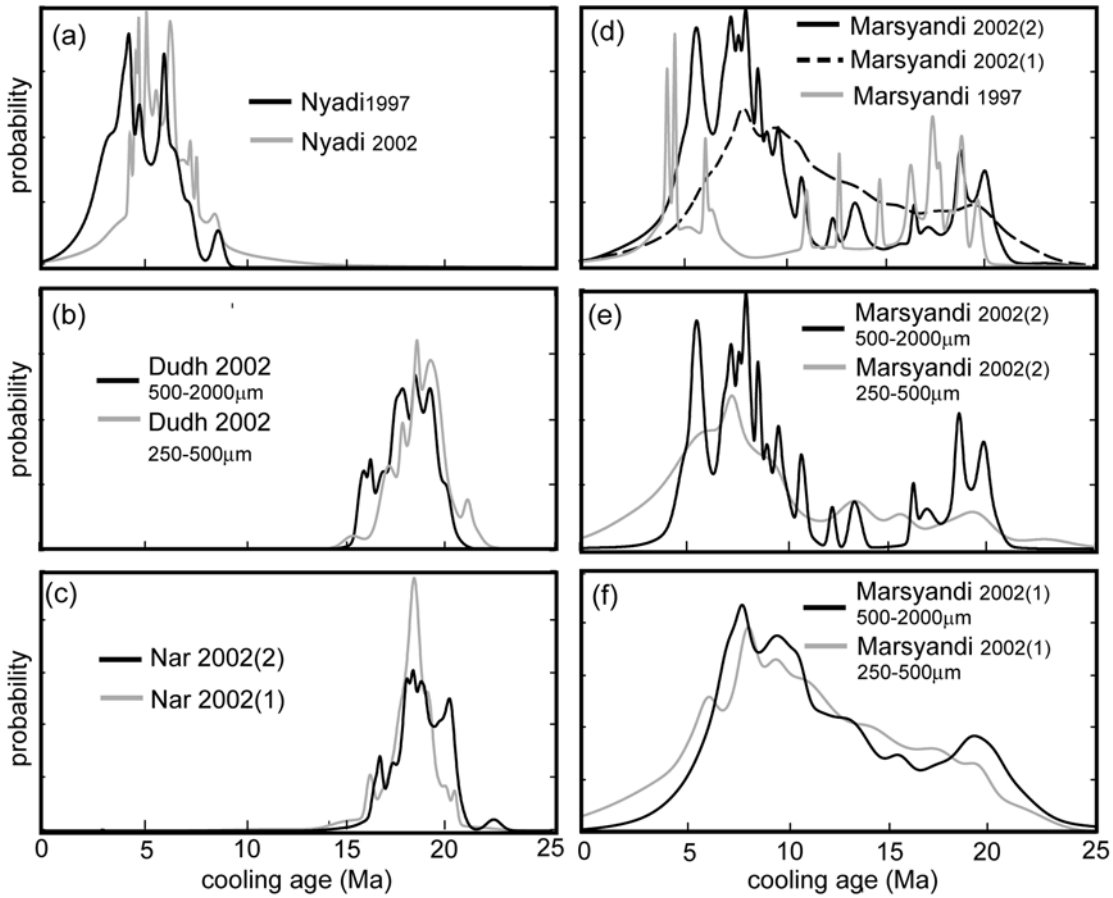

Figure 3. Muscovite $^{40}Ar/^{39}Ar$ cooling age SPDF comparisons. See Table 1 for summary of statistical comparison results. Area under each curve is normalized to unity. SPDFs for Marsyandi tributary sample results: (a) collected in Nyadi catchment 5 years apart, (b) collected in the Dudh catchment for comparison of different grain size fractions, and (c) collected from nearby locations in Nar catchment. SPDFs for Marsyandi River trunk stream samples: (d) Marsyandi 2002(2) 250–2000 μm, Marsyandi 2002(1) 250–2000 μm, and Marsyandi 1997 [*Brewer et al.*, 2005], collected at nearby locations in 1997 and 2002, (e) Marsyandi 2002(2) curves for 250–500 μm and 500–2000 μm grain size fractions, and (f) Marsyandi 2002(1) curves for 250–500 μm and 500–2000 μm grain size fractions.

Canada. Values for the irradiation parameter *J* were determined using Taylor Creek sanidine at 28.34 Ma [*Dalrymple and Duffield*, 1988; *Renne et al.*, 1998] as the flux monitor. Corrections for interfering reactions were measured using a combination of synthetic and natural salts [see *Kirby et al.*, 2002].

[18] Previously published step heating $^{40}Ar/^{39}Ar$ experiments on bedrock muscovites from the detrital muscovite source region in this part of the Himalaya [e.g., *Copeland et al.*, 1991; *Macfarlane*, 1993; *Edwards*, 1995], as well as our own unpublished experiments, show no discernable evidence of excess ^{40}Ar contamination. As a consequence, we decided that single-grain total fusion analyses, rather than more time-consuming incremental heating studies of individual crystal, would provide sufficiently reliable indications of bulk closure ages. Thus, after being baked out under vacuum at 250–300°C for a minimum of 8 hours, samples were individually fused with a defocused Ar-ion laser beam at a power level of ~15 W for 15 s. After purification with SAES St101 and St172 getters, Ar isotopic ratios were measured on an MAP 215–50 mass spectrometer using an electron multiplier detector and blank corrected.

[19] Dates for each grain were determined and 2σ apparent age uncertainties were assigned using the program ArArCALC version 2.2 [*Koppers*, 2002]. The data are reported in Table A of the auxiliary material[1], where 2σ uncertainties are shown with and without contributions from the uncertainty in the irradiation parameter *J*. Apparent age PDFs (equation (2a)) were constructed for each grain based on the uncertainties without *J* contributions and assuming a Gaussian distribution of error. The SPDF for each detrital sediment sample was determined by summing the PDFs for all grains analyzed from the sample and normalizing the result (equation (2b)). In order to compare the $^{40}Ar/^{39}Ar$

[1] Auxiliary material is available at ftp://ftp.agu.org/apend/tc/2004TC001712.

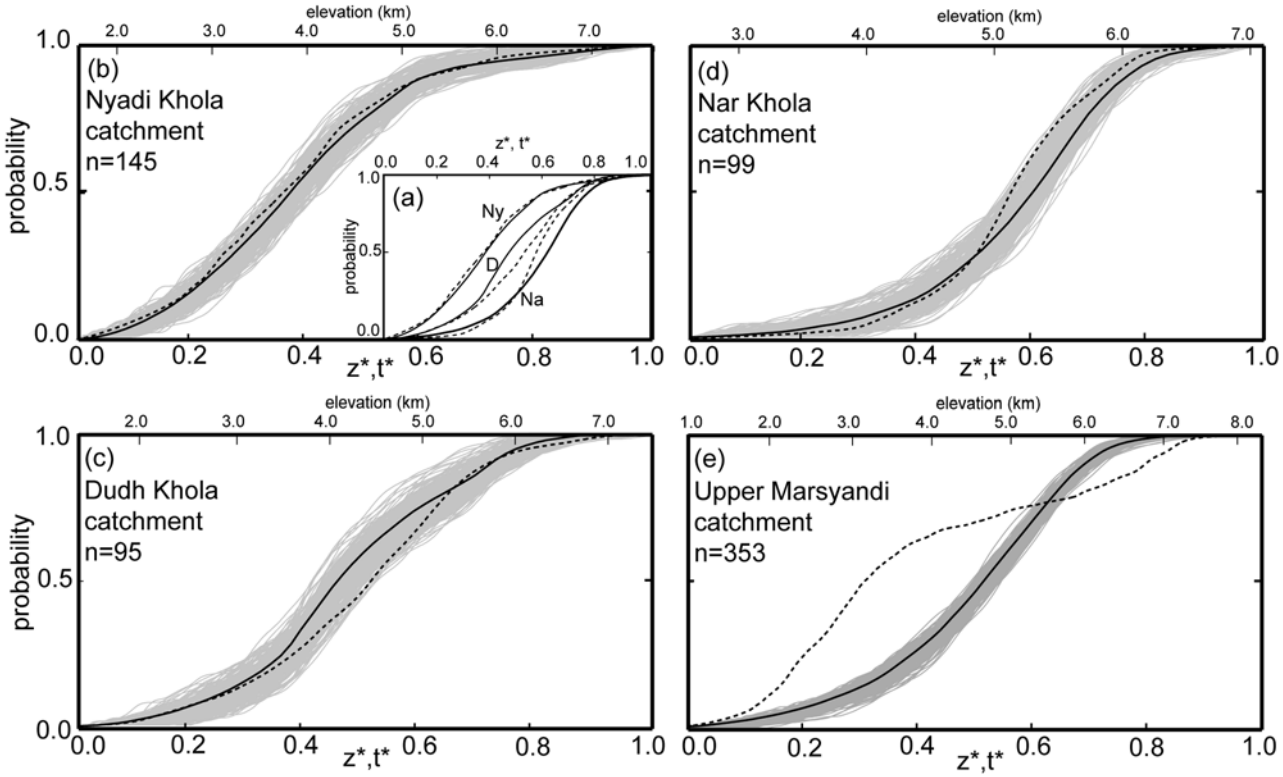

Figure 4. Comparison of cumulative hypsometric curves $CSPDF_{z^*}$ (solid black lines) and cooling age $CSPDF_{t^*}$ curves (dashed black lines). (a) Overlay of Nyadi curves "Ny," Dudh curves "D", and Nar curves "Na." Note lack of overlap in z*,t* probability space for the three data sets. $CSPDF_{t^*}$ versus $CSPDF_{z^*}$ comparisons for the (b) Nyadi catchment, (c) Dudh catchment, (d) Nar catchment, and (e) upper Marsyandi catchment, where n is the number of $^{40}Ar/^{39}Ar$ analyses represented by the cooling age CSPDF. See text for description of the 300 model $CSPDF_{t^*m}$ curves plotted for each catchment (gray curves).

data and hypsometric data more effectively, these are plotted as cumulative SPDFs (CSPDFs), which represent the probability that the age takes on a value less than or equal to t:

$$\mathrm{CSPDF} = \sum_{j=0}^{t} \mathrm{SPDF}(j) \tag{4}$$

4. Results

[20] Figure 3 shows cooling age SPDFs for detrital muscovite $^{40}Ar/^{39}Ar$ data from the sample sites. Individual muscovite cooling ages ranged from ~2 to 22 Ma, with a general trend of older ages (~15 to 20 Ma) for catchments to the north and younger ages (~3 to 10 Ma) for catchments to the south, consistent with the N-S gradient in erosion/uplift rates inferred by *Brewer et al.* [2005]. In light of the limited sizes of the Nyadi, Dudh, and Nar catchments, our expectation was that cooling age CSPDFs for samples from these catchments would simply match the shape of the appropriate hypsometric curves as predicted by a steady state model. Instead, we found a range of data behaviors, with the Nyadi catchment being the simplest to interpret and the Dudh and Nar catchments being more complicated. As expected, samples from the Marsyandi River itself yielded the most complex cooling age signals.

4.1. Nyadi Khola

[21] The Nyadi Khola catchment hypsometry, shown in Figures 2b and 4b, spans a total catchment relief of R = 6.2 km. Cooling age SPDFs are shown in Figure 3a for two detrital samples from the catchment. The first curve, Nyadi 1997 (the number indicates the year in which it was collected), represents 34 $^{40}Ar/^{39}Ar$ analyses for grains ranging in size from 500 to 2000 μm [*Brewer et al.*, 2005]. The second curve, Nyadi 2002, which we collected from a similar position in the catchment, represents 111 muscovite crystals within the same size range. In detail, the SPDFs look different. The 2002 curve tails off to somewhat older apparent ages. The 1997 sample curve has a higher concentration of grains with younger apparent ages and is generally smoother due to lower analytical precision. In order to compare the two curves in a statistically rigorous way, we applied a variant of the Kolmogorov-Smirnov (K-S) test. Unlike the original K-S test, which is relatively insensitive to the tails of distributions, this variant,

Table 1. Kuiper Equality Test Results (alpha = 0.05) for Selected Combinations of Cooling Age SPDFs[a]

Sample 1	n1	Sample 2	n2	V	P	H
Dudh, 250–500 μm	49	Dudh, 500–2000 μm	46	0.210	0.733	1
Nar 2002 (1), 500–2000 μm	50	Nar 2002(2), 500–2000 μm	49	0.196	0.806	1
Nyadi 1997, 500–2000 μm	34	Nyadi 2002, 500–2000 μm	111	0.238	0.399	1
Marsyandi 2002(2), 250–500 μm	70	Marsyandi 2002(2), 500–2000 μm	73	0.160	0.837	1
Marsyandi 2002(1), 250–500 μm	85	Marsyandi 2002(1), 500–2000 μm	77	0.078	0.999	1
Marsyandi 2002(1), 250–2000μm	162	Marsyandi 2002(2), 250–2000 μm	143	0.229	0.008	0
Marsyandi 2002(1), 250–2000μm	162	Marsyandi 1997, 500–2000 μm	48	0.348	0.003	0
Marsyandi 2002(2), 250–2000μm	143	Marsyandi 1997, 500–2000 μm	48	0.393	0.000	0

[a]Kuiper statistic V and the significance level P of an observed value of V are calculated for each comparison between sample 1 defined by n1 analyses and sample 2 defined by n2 analyses (as a disproof of the null hypothesis that the cooling age distributions are the same). H = 1 indicates that null hypothesis cannot be disproved at significance level alpha; H = 0 indicates that samples 1 and 2 are different at significance level alpha.

the two-sample Kuiper test [*Kuiper*, 1962; *Stephens*, 1965; *Press et al.*, 1992] guarantees equal sensitivities at all age values (t_m). For two cumulative distribution functions $S_1(t_m)$ and $S_2(t_m)$ made up of n_1 and n_2 observations, respectively, the Kuiper statistic (V) is the sum of the maximum distance of $S_1(t_m)$ above and below $S_2(t_m)$:

$$V = \max_{-\infty<t_m<\infty}[S_1(t_m) - S_2(t_m)] + \max_{-\infty<t_m<\infty}[S_2(t_m) - S_1(t_m)] \quad (5)$$

with

$$Q_{KP}(\lambda) = 2\sum_{j=1}^{\infty}\left(4j^2\lambda^2 - 1\right)e^{-2j^2\lambda^2} \quad (6a)$$

which satisfies

$$Q_{KP}(0) = 1,\ Q_{KP}(\infty) = 0 \quad (6b)$$

In terms of this function, P, the significance level of an observed value of V (as a disproof of the null hypothesis that the distributions are the same) is

$$P(V > \text{observed}) = Q_{KP}\left\{\left[\sqrt{N_e} + 0.155 + 0.24/\sqrt{N_e}\right]V\right\} \quad (7)$$

with

$$N_e = \frac{n_1 n_2}{n_1 + n_2} \quad (8)$$

Comparisons for which $P > 0.05$ are consistent with $S_1(t_m)$ and $S_2(t_m)$ being equal at the 95% significance level. Kuiper test statistics for the comparisons used in this study are summarized in Table 1. In this instance, $V = 0.24$, and $P = 0.40$. Because this result is consistent with the age signals from Nyadi 1997 and Nyadi 2002 being statistically indistinguishable, we conclude that the apparent mismatch in Figure 3a can be explained simply by differences in analytical precision and in the number of muscovites analyzed from the 1997 and 2002 samples.

[22] In order to evaluate the steady state assumption, we began by normalizing the apparent ages (t_m) and the elevations (z) for each probability distribution using dimensionless age, t^*, and dimensionless elevation, z^*, so that z^* and t^* each range between 0 and 1:

$$t^* = \frac{(t_m - t_{m_{\min}})}{t_{\text{range}}} \quad (9a)$$

$$z^* = \frac{(z - z_{\min})}{R} \quad (9b)$$

where $t_{m_{\min}}$ and $z_{\min}$ are the minimum cooling age and elevation, respectively. The hypsometric curve calculated using z^*, CSPDF_{z^*}, is then a plot of normalized elevation versus normalized cumulative area [e.g., *Strahler*, 1952; *Brocklehurst and Whipple*, 2004].

[23] The formal definition of t_{range} as the difference between the oldest and youngest measured age for a sample implies a value of 13.5 Myr for the combined Nyadi 1997 and Nyadi 2002 data sets ($n = 145$). However, the practical application of this definition is complicated by the relatively large uncertainties frequently encountered for extremely young grains that can define the tails of cooling age SPDFs for detrital samples from active orogenic systems. A more robust approach is to assign a value to t_{range} such that (1) the interval comprises 99% of the area under the cooling age SPDF and (2) the assigned value minimizes the mismatch between the shapes of the discretized t^* and z^* curves. For the combined Nyadi data sets, this approach yields a value of 8.5 Myr for t_{range}. Using this value to discretize t^*, and the catchment relief ($R = 6.2$ km) to discretize z^*, we plotted the resulting CSPDF_{t^*} curve and the corresponding hypsometric curve CSPDF_{z^*} in Figures 4a and 4b. Again, the two Nyadi curves show some differences, but are these differences significant?

[24] As it happens, neither the Kuiper test nor the original K-S test is a particularly useful diagnostic for comparing these dimensionless distributions. The reason lies in the very large number of precise elevation data used to define the hypsometric curve ($n = 2.4 \times 10^4$). As a consequence, the value of N_e for the Kuiper test is also very large and V and P reach their limiting values of 1 and 0, making comparisons between the CSPDF_{t^*} and CSPDF_{z^*} curves inevitably unfavorable at the 95% significance level. To explore the effects of sample and catchment size more

effectively, we addressed the question of mismatch significance by constructing a model $CSPDF_{t^*}$ curve ($CSPDF_{t^*m}$) from n points randomly selected from the corresponding $CSPDF_{z^*}$ distribution, where n is the number of grains analyzed from the sample. This process was repeated 300 times to define a family of $CSPDF_{t^*m}$ curves that describes the reasonable range of deviation from the $CSPDF_{z^*}$ curve that would be expected for a sample of size n. The results of this exercise are illustrated in Figure 4b. $CSPDF_{t^*}$ lies well within the range of $CSPDF_{t^*m}$ curves, implying that the topologies of the cooling age and hypsometric distributions are consistent with steady state assumptions. As a consequence, we consider ~0.7 km/Myr, calculated using equation (1), with t_{range} = 8.5 Myr and R = 6.2 km, to be a reasonable estimate of the time-averaged erosion rate for the catchment over the 11–2.5 Ma interval.

4.2. Dudh Khola

[25] The Dudh Khola catchment hypsometry spans a total relief of R = 5.7 km (Figures 2c and 4c). Cooling ages ranging between ~15 and 22 Ma were obtained for coarse (500–2000 μm) and fine (250–500 μm) Dudh Khola muscovites. Comparison of the coarse-grained SPDF (n = 46) and fine-grained SPDF (n = 49) using the Kuiper test yields V = 0.21 and P = 0.73, indicating that the two SPDFs agree at the 95% level of confidence (Figure 3b). Thus there is no clear bias between the signals provided by coarse and fine grain size fractions, suggesting that both are similarly representative of bedrock cooling ages throughout the catchment. The t_{range} calculated from the best fit hypsometric curve comparison that incorporates 99% of the area under the age SPDF for the full range of grain sizes (n = 95) is 6.9 Myr. On the basis of the total catchment relief and this estimate for t_{range}, steady state assumptions would imply a uniform erosion rate of ~0.8 km/Myr. As we did for the Nyadi Khola data set, we normalized the age distribution using this t_{range}, normalized the hypsometric distribution using R (equations (9a) and (9b)), and plotted the corresponding modeled $CSPDF_{t^*m}$ curves, each constructed from n = 95 points randomly selected from the hypsometric curve. The Dudh Khola $CSPDF_{t^*}$ curve (n = 95) is displaced toward older ages with respect to the hypsometric $CSPDF_{z^*}$ curve at elevations from ~3 to 5 km (Figure 4c), but lies just within the probability space covered by 300 model $CSPDF_{t^*m}$ curves. As a consequence, we cannot disprove the hypothesis that steady state conditions were met. However, very few model runs deviate more significantly from the expected trend than the measured $CSPDF_{t^*}$ curve, so that the probability that the two curves are consistent with the steady state hypothesis is low. The relatively poor match implies a degree of nonrepresentative sampling of the catchment's full relief or some deviation from steady state conditions, and we must view the ~0.8 km/Myr rate with skepticism.

4.3. Nar Khola

[26] The Nar Khola catchment spans a total relief of R = 4.5 (Figures 2d and 4d). A pair of detrital muscovite samples collected at nearby locations in the catchment were analyzed in order to extend the limited spatial scale (tens of meters) and number of analyses (n = 37 total for two samples) used for a similar comparison by *Brewer et al.* [2005]. Comparison of SPDFs for samples Nar 2002(1) (500–2000 μm, n = 49) and Nar 2002(2) (500–2000 μm, n = 50), collected ~4 km apart in the Nar Khola, yields V = 0.20 and P = 0.80 over the narrow age range of ~15 to 22 Ma, indicating that the two SPDFs are statistically indistinguishable, and suggesting that the sediment is well mixed (Figure 3c).

[27] The value of t_{range} calculated from the best fit hypsometric curve for the full range of Nar Khola grain sizes (n = 99) is 9.9 Myr, implying an apparent erosion rate of ~0.5 km/Myr. The $CSPDF_{t^*}$ curve calculated from the combined thermochronologic data sets (n = 99) matches the $CSPDF_{z^*}$ curve well below ~5 km but departs from the predicted trend at higher elevations (Figure 4d). Synthetic $CSPDF_{t^*m}$ curves define a probability space that just barely includes $CSPDF_{t^*}$. As a consequence, there is very little chance that the cooling age distribution faithfully mimics the catchment's hypsometry, and thus any nominal apparent erosion rate based on the erosion model assumed here and by *Brewer et al.* [2005] is not likely to be reliable.

4.4. Marsyandi Trunk Stream Samples

[28] Marsyandi trunk stream samples collected between the Khudi Khola and Nyadi Khola tributary junctions represent 2590 km^2 of drainage area spanning elevations from 850 to 8150 m (R = 7.3 km) in the upper Marsyandi catchment (Figures 2a and 2e). In anticipation of the complex cooling age signal we would expect from a trunk stream like the Marsyandi, we analyzed a large number of micas from two samples collected 2 km apart: Marsyandi 2002(1) (250–2000 μm, n = 162) and Marsyandi 2002(2) (250–2000 μm, n = 143). These samples were collected from the same area as the Marsyandi 1997 trunk stream sample collected by I. D. Brewer et al. (500–2000 μm, n = 48), and the 305 new dates span the range ~2 to ~22 Ma.

[29] Kuiper statistics for all Marsyandi sample comparisons indicate that comparisons between pairs of samples collected in nearby locations are not favorable at the 95% confidence level (Table 1 and Figures 3d–3f). For example, the Kuiper test for the comparison between Marsyandi 2002(1) (250–2000 μm, n = 162) and Marsyandi 2002(2) (250–2000 μm, n = 143) yields V = 0.23 and P = 0.01, indicating that the two age distributions are significantly different. Kuiper test results are consistent both with the fine (250–500 μm) and coarse (500–2000 μm) size fractions from Marsyandi 2002(1) being indistinguishable and with the fine and coarse size fractions from Marsyandi 2002(2) being indistinguishable, which suggests that it is appropriate to compare the combined (250–2000 μm) Marsyandi samples from 2002 with each other and with the (500–2000 μm) sample from 1997 (Figure 3d).

[30] Although the inconsistencies between the sets of paired nearby samples collected in different years and in the same year (Table 1) imply that sediment samples from such a large catchment do not represent the full distribution

of bedrock ages with high fidelity, and are simply unreliable for erosion rate calculations, we carried out the analysis, as for the previous catchments, for completeness. For the combined Marsyandi data set (n = 353), the best fit hypsometric curve comparison implies a t_{range} of 24.5 Myr and a nominal erosion rate for the entire catchment of ~0.3 km/Myr. As expected, the $CSPDF_{t*}$ curve departs significantly over the entire elevation range from the trend predicted by 300 synthetic $CSPDF_{t*m}$ curves (Figure 4e).

5. Discussion and Conclusions

[31] Our results from the Marsyandi River and its tributaries illustrate how comparative $^{40}Ar/^{39}Ar$ data sets and hypsometric curves for a particular catchment can be used to test the critical hypotheses involved in erosion rate modeling. Comparisons of cooling age SPDFs for nearby samples, different grain size fractions of the same sample, and samples collected in different years can be interpreted in a straightforward way to determine how well a sample represents a catchment's erosional signal. Most important, however, is the comparison of cooling age CSPDFs and hypsometric curves. Because agreement between these curves is only expected if all model, sampling, and steady state assumptions hold, such comparisons are a straightforward way to identify appropriate catchments for erosion rate modeling.

5.1. Representative Sedimentary Signal and Uniform Erosion

[32] Agreement among age distributions for nearby samples is expected if point source preferential erosion is insignificant. Good agreement for the Nar Khola catchment samples, Nar 2002(1) and Nar 2002(2) (Figure 3c and Table 1) and for the Nyadi Khola samples collected in 1997 and 2001 (Figure 3a and Table 1), indicate that this model requirement is likely to be met in this region over drainage areas on the order of 200–940 km^2. In contrast, the same conclusions do not hold for nearby samples collected from the trunk stream (Table 1). Although the discrepancy between the two distributions may be attributable to undersampling of a complex signal, we note that much of the mismatch is caused by a peak at ~5 Ma in Marsyandi 2002(2) that is not present in the Marsyandi 2002(1) sample (Figure 3d). This suggests that preferential erosion of point sources like landslides or temporary sediment storage may be problematic at this large catchment scale (2590 km^2) and therefore that the sizes of the Marsyandi River tributary catchments, not the trunk stream catchment, may be the largest appropriate scale for modeling erosion histories in the study area.

[33] Low mismatches for SPDF comparisons of fine and coarse grain sizes are expected for small catchments that integrate areas with restricted lithologic variation and little spatial variation in erosion rate. An example of this behavior may be found in the data sets for the Dudh Khola catchment (Figure 3b). Alternatively, the same low mismatch may result if the fine-grained micas are mainly fragments of the same coarse-grained micas that make up the 500–2000 μm fraction. The same behavior was observed in the Marsyandi 2002 (1,2) data sets (Figures 3e and 3f and Table 1), even though the catchment exhibits strong N-S gradients in cooling age and muscovite abundance, and is likely to be affected by complicated patterns of active faulting since the Pliocene [e.g., *Edwards*, 1995; *Hodges et al.*, 1996; *Coleman and Hodges*, 1998; *Hodges*, 2000; *Catlos et al.*, 2001; *Hodges et al.*, 2004]. Given this lithologic and erosional heterogeneity, the lack of a clear bias between the signals provided by the Marsyandi coarse and fine grain size fractions suggests that grain fragmentation rather than uniform erosion and muscovite distribution is responsible for the good agreement. Either way, the results indicate that our ability to characterize a catchment's cooling age signal is not hindered by limiting the range of grain sizes analyzed.

[34] Significant sediment storage and influences from local point sources like landslides could be expected to cause sedimentary signal variation at a particular location from year to year. Favorable equality test results for samples collected 5 years apart suggests that these influences are not problematic in the Nyadi Khola catchment (Figure 3a and Table 1). Importantly, the good comparison also suggests that the data are not strongly biased by an individual researcher's sampling site selection. The same conclusions do not hold for the Marsyandi catchment as a whole, probably because the samples may be overwhelmed by local sediment sources or the effects of temporary tributary blockage and are not fully representative of the bedrock cooling ages in this large catchment.

[35] *Vermeesch* [2004] outlined a method for calculating the smallest number of grains in a sample that must be dated to achieve a desired level of statistical adequacy, assuming the worst-case scenario, that the catchment ages form a perfectly uniform distribution where each age fraction is the same size. In most cases, we have performed enough analyses such that no significant fraction of the worst-case scenario population is missed at the 95% confidence level (e.g., Table 2). However, natural age populations are expected to differ from this worst-case population, such that fewer grains may be needed to reach the desired level of statistical adequacy [*Vermeesch*, 2004]. Our favorable empirical comparisons for SPDFs collected in the Nar, Dudh and Nyadi catchments indicate that ~45 to 50 analyses for each sample may adequately characterize these simple tributary catchments. Additionally, agreement between SPDF comparisons characterized by only ~70–85 analyses for different grain size fractions collected from the more complicated Marsyandi River catchment suggest that limited sample size is not responsible for the mismatch between paired nearby Marsyandi River samples.

5.2. Steady State Assumptions and Erosion Rate Estimates

[36] In general, a large mismatch between $CSPDF_{t*}$ for a detrital sample and $CSPDF_{z*}$ for the catchment from which it was collected is inconsistent with uniform erosion and with the thermal structure and topography being at steady

Table 2. Maximum Likelihood P_{max} of Missing a Fraction of the Worst-Case Scenario Cooling Age Population[a]

Sample	*n*	P_{max}, %							
		f = 0.01	f = 0.02	f = 0.03	f = 0.04	f = 0.05	f = 0.06	f = 0.07	f = 0.08
Nyadi Khola catchment (all)	145	100	95	34	7	1	0	0	0
Dudh Khola catchment (all)	95	100	100	87	42	14	4	1	0
Nar Khola catchment (all)	99	100	100	84	37	12	3	1	0
Upper Marsyandi catchment (all)	353	95	4	0	0	0	0	0	0

[a]Corresponding to more than *f* of the total is missed at the 95% significance level, given the number of $^{40}Ar/^{39}Ar$ analyses *n* performed for each sample, after the method of *Vermeesch* [2004, see http://pangea.stanford.edu/research/noble/provenance].

state over the length and timescales represented by the detrital data set. A small, but finite, probability exists that the discrepancy between the Dudh Khola $CSPDF_{t*}$ and $CSPDF_{z*}$ is caused by small sample size ($n = 95$), and that the cooling age curve matches the hypsometric curve well enough to be consistent with these conditions. If this is true, our calculated apparent erosion rate of ~0.8 km/Myr, similar to the rate of 0.94 km/Myr modeled by *Brewer et al.* [2005], is appropriate over the ~20 to 15 Ma interval. However, because the $CSPDF_{t*}$ lies at the limit of the parameter space predicted to be consistent with steady state, it is likely that the mismatch between the curves could result from something other than low sampling density, and that the erosion rate calculated above is not robust.

[37] Another potential cause of such a mismatch might be a nonuniform distribution of muscovite, since the bedrock in the catchment consists of a variety of gneisses, weakly metamorphosed carbonate rocks, and granites. The magnitude of this problem could be addressed through point-counting studies at different locations within the Dudh Khola catchment. Temporary sediment storage or recent preferential erosion of temporarily stored material derived from high elevations (e.g., glacial deposits or landslides) also may have caused the sample to represent some elevations preferentially. This possibility could be evaluated through systematic geomorphic mapping of the catchment. A third influence may be deformation in the catchment during the closure interval of ~20–15 Ma. For example, one or more strands of the South Tibetan Fault system (STFS, Figure 2a) transect the catchment [*Coleman and Hodges*, 1998; *Searle and Godin*, 2003], and there is good evidence for post-middle Miocene activity on the STFS in other parts off the Annapurna Range [*Hodges et al.*, 1996; *Hurtado et al.*, 2001]. This possibility could be explored by collecting bedrock thermochronologic samples from traverses on either side of the fault in order to establish whether or not long-term erosion rates vary across it. Detrital thermochronology and hypsometric analysis from smaller tributary catchments within the Dudh Khola catchment also could be used to investigate uniform erosion and steady state assumptions at a smaller spatial scale.

[38] As was the case for the Dudh Khola, a small probability exists that the cooling age and hypsometric curves are consistent with steady state in the Nar Khola. If the model conditions are indeed satisfied, we calculate an apparent erosion rate of ~0.5 km/Myr for the period represented by the samples, ~20 to 15 Ma. However, this interpretation must be viewed with considerable skepticism given the poor comparative statistics. Structural activity, transient topography and spatially variable erosion, heterogeneous thermochronometer distribution, or simply our inability to sample the bedrock cooling age signal over a large drainage area are possible explanations for the mismatch. The Nar Khola drains metacarbonate rocks and granites with varying muscovite abundances, and may have experienced short-term fluctuations in sediment mixing and delivery to a particular sample location. In order to test these hypotheses, spatial variations in erosion rate must be examined through bedrock thermochronologic studies and comparisons of cooling age and hypsometric distributions for subcatchments within the greater Nar Khola catchment. Regardless of the reason for the mismatch, the unfavorable comparison between the age signal and hypsometric curve shapes indicate that neither the erosion rate calculated here nor the rate of 1.12 km/Myr modeled by *Brewer et al.* [2005] is robust.

[39] While the cooling age-elevation relationships inferred from the detrital age signals in the Nar and Dudh Khola catchments allow us to estimate apparent erosion rates for the period ~20 to 15 Ma, the Nyadi Khola catchment detrital signal yields information about the period from ~11 to 2.5 Ma. The excellent match between $CSPDF_{z*}$ and $CSPDF_{t*}$ for the large ($n = 145$) Nyadi Khola data set is consistent with steady state assumptions for this small catchment and implies that our maximum apparent erosion rate of ~0.7 km/Myr may be robust for this period. This estimate differs significantly from the 2.3 km/Myr rate modeled by *Brewer et al.* [2005]. Although the two studies differ in the number of grains analyzed, the difference between the cooling age SPDFs for the Nyadi samples is not statistically significant, so the discrepancy in estimated rate does not derive from the use of significantly different data sets. Instead, the inconsistency reflects a fundamental difference in the time period over which each method averages the rate. If the *Brewer et al.* [2003] approach is analogous to combining a single bedrock cooling age from the average elevation in a catchment and a thermal model to estimate average *E* since closure of the bulk of the catchment's bedrock [e.g., *Hodges*, 2003], our approach is analogous to using a bedrock age-elevation transect to estimate an apparent erosion rate for the time over which the samples passed through the closure isotherm [e.g., *Wagner and Reimer*, 1972].

[40] Specifically, *Brewer et al.* [2005] calculated a vertical steady state erosion rate by finding the lowest mismatch between the Nyadi 1997 data and a theoretical cooling age SPDF based on modeled isotherm depth (z_c), catchment hypsometry, relief and erosion rate. For a rate of 2.3 km/Myr, the model predicts a theoretical SPDF centered at ~5 Ma. Although this mean age matches the mean of the sample distribution, the total range of cooling ages in the catchment (predicted to be <3 Myr for an erosion rate of 2.3 km/Myr) is a very poor fit to the data. On the other hand, our estimated exhumation rate of ~0.7 km/Myr seems inadequate to explain cooling ages as young as 2.5 Ma for any reasonable geothermal gradient. In all likelihood, the data imply an increase in the rate of exhumation over the last 2.5 Myr to substantially more than the 2.3 km/Myr estimate provided by the method of Brewer et al. for the interval ~5 Ma to the present. A full reconstruction of the time-temperature history of the catchment would require a systematic study of bedrock thermochronology involving multiple mineral-isotopic systems.

[41] When considering only the uniform steady state vertical erosion model used here and by *Brewer et al.* [2005], we argue that our approach is generally more reliable for estimating apparent erosion rates during the closure interval because (1) we use considerably more information than the mean of the age distribution in arriving at and testing an optimal model and (2) our calculation does not require us to assume a specific thermal structure, only that this structure does not change significantly through time. This latter attribute is particularly advantageous for the study of young, rapidly exhuming orogenic terrains where the thermal structure can be complex. Our approach is not well suited for studies in which small detrital sample size or very large analytical errors make it difficult to estimate t_{range} and characterize bedrock cooling ages well enough to test the restrictive set of model assumptions; if more high-precision analyses cannot be done, a thermal modeling approach may be better, even though it provides no way to evaluate the model assumptions.

5.3. Problem of Nonvertical Exhumation Paths

[42] Both our approach and that of I. D. Brewer and colleagues presume that exhumation simply involves the erosion of overburden and vertical transport of the source region of a detrital mica sample from the depth of the closure isotherm to the surface (Figure 1a). In real orogenic systems, this is likely to be almost never strictly the case. The lateral advection of heat and rock results in quite complex temperature-time trajectories [e.g., *Batt and Braun*, 1997; *Huerta et al.*, 1998; *Ehlers and Farley*, 2003]. In general, we might suspect that the erosion rates calculated with our method or that of I. D. Brewer and colleagues underestimate the true rate of rock advection toward the surface, but it is difficult to predict the magnitude of the effect without numerous assumptions regarding deformational kinematics and the concentration and distribution of heat-producing elements in the region. We are presently involved in efforts to explore the possible effects of heat and rock transport in the Marsyandi area in much greater detail, through three-dimensional thermokinematic modeling. For the time being, we note that the absolute values for erosion rate estimated with "one-dimensional" approaches such as those described here are less valuable than the sense of variability of apparent erosion rates from one catchment to another over specific time intervals. Such information can provide important insight regarding regional exhumation patterns through time. In addition, the methods introduced here constitute a simple and powerful way to explore the probability that specific catchments maintained steady state conditions over a specific time frame. For example, our analysis of the Nyadi Khola data implies that the catchment of this river did indeed approach erosional and thermal steady states over the 11 to 2.5 Ma interval.

6. Summary

[43] The use of detrital mineral cooling ages from modern sediments to infer regional patterns in erosion rate is advantageous because it compliments the spatial extrapolation of bedrock cooling histories, samples are easy to collect in areas where bedrock sampling is difficult, and automated single-grain $^{40}Ar/^{39}Ar$ analyses are both time and cost efficient. Our technique for calculating an apparent erosion rate from a detrital sample's cooling age range and the total relief of the contributing drainage area is analogous to determining the catchment's bedrock cooling age-elevation gradient over the closure interval of the sampled minerals. Like the bedrock age-elevation proxy for erosion rate, our approach is also advantageous because it does not require the assumption of a particular thermal structure as the previous model of *Brewer et al.* [2003, 2005] does.

[44] However, the value of such analyses hinges on our ability to evaluate the many assumptions that remain inherent in the technique, most importantly, that steady state conditions must have been met during the closure interval recorded by the detrital mineral dates, and that the full range of bedrock cooling dates in the catchment must be represented by the analyzed grains in the sediment sample. We have described in this paper how comparisons of catchment hypsometry and the shape of the detrital cooling age signal using normalized CSPDF curves can help with this evaluation. Only if these assumptions hold for a uniformly eroding catchment in which bedrock cooling ages are sampled in proportion to area do we expect these curves to coincide.

[45] Comparisons of detrital muscovite $^{40}Ar/^{39}Ar$ age distributions and hypsometric curves for the corresponding catchments in the Marsyandi Valley imply that steady state assumptions do not apply over the necessary spatial and temporal scales for every drainage in this sector of the central Nepalese Himalaya. The Nyadi Khola catchment is a notable exception in that it showed a strong correlation of hypsometry and cooling age CSPDF. We calculated a maximum apparent erosion rate of ~0.7 km/Myr over the interval ~11 to 2.5 Ma. This result and the young average $^{40}Ar/^{39}Ar$ muscovite age of the sample (~5 Ma) imply an increase in erosion rate since the closure interval.

[46] A persistent problem in detrital cooling age studies is whether or not a sample adequately represents the full distribution of bedrock cooling ages in the sediment source region. In the Marsyandi region, we explored sampling fidelity by comparing SPDFs for nearby samples, different grain size fractions, and samples collected in different years. In this instance, we found that ~50 analyses were adequate to characterize the cooling age signal for tributary catchments with simple erosional histories, and that the sedimentary signal appears to be a high-fidelity record of the bedrock ages in these catchments. Comparisons in the upper Marsyandi catchment itself indicate that although ~70–85 grains may be sufficient to characterize a sample's age signal, these signals vary significantly at the kilometer scale and from year to year and are inappropriate for erosion rate modeling.

[47] **Acknowledgments.** We would like to thank our guides from Himalayan Experience and Taylor Schildgen for field assistance, Bill Olszewski and Malcolm Pringle for their expertise in the lab, and Pringle, Kelin Whipple, and Simon Brocklehurst for useful discussions regarding detrital thermochronology, hypsometric analysis, and the application of these tools to active orogenic systems. The paper benefited greatly from thoughtful reviews by Doug Burbank, Lothar Ratschbacher, and an anonymous reader. This work is a product of the NSF Continental Dynamics project "Geomorphic-Geodynamic Coupling at the Orogen Scale."

References

Adams, C. J., and S. Kelley (1998), Provenance of Permian-Triassic and Ordovician metagraywacke terranes in New Zealand: Evidence from $^{40}Ar/^{39}Ar$ dating of detrital micas, *Geol. Soc. Am. Bull.*, *110*, 422–432.

Batt, G. E., and J. Braun (1997), On the thermomechanical evolution of compressional orogens, *Geophys. J. Int.*, *128*, 364–382.

Bernet, M., M. Zattin, J. I. Garver, M. T. Brandon, and J. A. Vance (2001), Steady-state exhumation of the European Alps, *Geology*, *29*, 35–38.

Bernet, M., M. T. Brandon, J. I. Garver, and B. Molitor (2004a), Fundamentals of detrital zircon fission-track analysis for provenance and exhumation studies with examples from the European Alps, in *Detrital Thermochronology: Provenance Analysis, Exhumation, and Landscape Evolution of Mountain Belts*, edited by M. Bernet and C. Spiegel, *Spec. Pap. Geol. Soc. Am.*, *378*, 25–36.

Bernet, M., M. T. Brandon, J. I. Garver, and B. Molitor (2004b), Downstream changes of Alpine zircon fission-track ages in the Rhône and Rhine rivers, *J. Sediment. Res.*, *74*, 82–94.

Brandon, M. T., and J. A. Vance (1992), Fission-track ages of detrital zircon grains: Implications for the tectonic evolution of the Cenozoic Olympic subduction complex, *Am. J. Sci.*, *292*, 565–636.

Brewer, I. D. (2001), Detrital-mineral thermochronology, investigations of orogenic denudation in the Himalaya of central Nepal, Ph.D. thesis, 181 pp., Pa. State Univ., State College.

Brewer, I. D., D. W. Burbank, and K. V. Hodges (2003), Modelling detrital cooling-age populations: insights from two Himalayan catchments, *Basin Res.*, *15*, 305–320.

Brewer, I. D., D. W. Burbank, and K. V. Hodges (2005), Downstream development of a detrital cooling-age signal: Insights from $^{40}Ar/^{39}Ar$ muscovite thermochronology in the Nepalese Himalaya, *Spec. Publ. Geol. Soc. Am.*, in press.

Brocklehurst, S., and K. Whipple (2004), Hypsometry of glaciated landscapes, *Earth Surf. Processes Landforms*, *29*, 907–926.

Brozovic, N., D. Burbank, and A. Meigs (1997), Climatic limits on landscape development in the northwestern Himalaya, *Science*, *276*, 571–574.

Bullen, M. E., D. W. Burbank, J. I. Garver, and K. Abdrakhmatov (2001), Late Cenozoic evolution of the northwestern Tien Shan: New age estimates for the initiation of mountain building, *Geol. Soc. Am. Bull.*, *113*, 1544–1559.

Carrapa, B., J. Wijbrans, and G. Bertotti (2003), Episodic exhumation in the western Alps, *Geology*, *31*, 601–604.

Catlos, E. J., T. M. Harrison, M. J. Kohn, M. Grove, F. J. Ryerson, C. E. Manning, and B. N. Upreti (2001), Geochronologic and thermobarometric constraints on the evolution of the Main Central Thrust, central Nepalese Himalaya, *J. Geophys. Res.*, *106*, 16,177–16,204.

Clift, P., A. Carter, and A. Hurford (1996), Constraints on the evolution of the East Greenland Margin: Evidence from detrital apatite offshore sediments, *Geology*, *24*, 1013–1016.

Colchen, M., P. Le Fort, and A. Pecher (1986), Annapurna–Manaslu–Ganesh Himal, pp. 75–136, Cent. Natl. de la Rech. Sci., Paris.

Coleman, M. E., and K. V. Hodges (1998), Contrasting Oligocene and Miocene thermal histories from the hanging wall and footwall of the South Tibetan detachment in the central Himalaya from $^{40}Ar/^{39}Ar$ thermochronology, Marsyandi Valley, central Nepal, *Tectonics*, *17*, 726–740.

Copeland, P., T. M. Harrison, K. V. Hodges, P. Maruéjol, P. LeFort, and A. Pêcher (1991), An early Pliocene thermal disturbance of the Main Central Thrust, central Nepal: Implications for Himalayan tectonics, *J. Geophys. Res.*, *96*, 8475–8500.

Dalrymple, G. B., and W. A. Duffield (1988), High precision $^{40}Ar/^{39}Ar$ dating of Oligocene rhyolites from the Mogollon-Datil volcanic field using a continuous laser system, *Geophys. Res. Lett.*, *15*, 463–466.

Edwards, R. M. (1995), $^{40}Ar/^{39}Ar$ geochronology of the Main Central Thrust (MCT) region: Evidence for late Miocene to Pliocene disturbances along the MCT, Marsyangdi River valley, west-central Nepal Himalaya, *J. Nepal Geol. Soc.*, *10*, 41–46.

Ehlers, T. A., and K. A. Farley (2003), Apatite (U-Th)/He thermochronometry: methods and applications to problems in tectonic and surface processes, *Earth and Planet. Sci. Lett.*, *206*, 1–14.

Fielding, E. J., B. L. Isacks, M. Barazangi, and C. Duncan (1994), How flat is Tibet?, *Geology*, *22*, 163–167.

Garver, J. I., M. T. Brandon, M. K. Roden-Tice, and P. J. J. Kamp (1999), Exhumation history of orogenic highlands determined by detrital fission track thermochronology, in *Exhumation Processes: Normal Faulting, Ductile Flow, and Erosion*, edited by U. Ring et al., *Geol. Soc. Spec. Publ.*, *154*, 283–304.

Hodges, K. V. (1998), $^{40}Ar/^{39}Ar$ geochronology using the laser microprobe, in *Applications of Microanalytical Techniques to Understanding Mineralizing Processes*, *Rev. Econ. Geol.*, vol. 7, edited by M. A. McKibben and W. C. Shanks III, pp. 53–72, Soc.of Econ. Geol., Tuscaloosa, Ala.

Hodges, K. V. (2000), Tectonics of the Himalaya and southern Tibet from two perspectives, *Geol. Soc. Am. Bull.*, *112*, 324–350.

Hodges, K. V. (2003), Geochronology and Thermochronology in orogenic systems, in *Treatise on Geochemistry*, vol. 3, *The Crust*, edited by R. L. Rudnick, pp. 263–292, Elsevier, New York.

Hodges, K. V., R. R. Parrish, and M. P. Searle (1996), Tectonic evolution of the central Annapurna Range, Nepalese Himalayas, *Tectonics*, *15*, 1264–1291.

Hodges, K., C. Wobus, K. Ruhl, T. Schildgen, and K. Whipple (2004), Quaternary deformation, river steepening, and heavy precipitation at the front of the Higher Himalayan ranges, *Earth Planet. Sci. Lett.*, *220*, 379–389.

Hodges, K. V., K. W. Ruhl, C. W. Wobus, and M. S. Pringle (2005), $^{40}Ar/^{39}Ar$ geochronology of detrital minerals, in *Thermochronology*, *Rev. Mineral. Geochem.*, edited by P. W. Reiners and T. A. Ehlers, Mineral. Soc. of Am., Washington, D. C., in press.

Huerta, A. D., L. H. Royden, and K. V. Hodges (1998), The thermal structure of collisional orogens as a response to accretion, erosion, and radiogenic heating, *J. Geophys. Res.*, *103*, 15,287–15,302.

Hurtado, J. M., K. V. Hodges, and K. X. Whipple (2001), Neotectonics of the Thakkhola Graben and implications for recent activity on the South Tibetan Fault System in the central Nepalese Himalaya, *Geol. Soc. Am. Bull.*, *113*, 222–240.

Kelley, S., and B. J. Bluck (1989), Detrital mineral ages from the southern Uplands using ^{40}Ar-^{39}Ar laser probe, *J. Geol. Soc. London*, *146*, 401–403.

Kirby, E., P. W. Reiners, M. A. Krol, K. X. Whipple, K. V. Hodges, K. A. Farley, W. Tang, and Z. Chen (2002), Late Cenozoic evolution of the eastern margin of the Tibetan Plateau: Inferences from $^{40}Ar/^{39}Ar$ and (U-Th)/He thermochronology, *Tectonics*, *21*(1), 1001, doi:10.1029/2000TC001246.

Koppers, A. P. (2002), ArArCALC software for $^{40}Ar/^{39}Ar$ age calculations, *Comput. Geosci.*, *28*, 605–619.

Kuiper, N. H. (1962), Tests concerning random points on a circle, *Proc. K. Ned. Akad. Wet., Ser. A*, *63*, 38–47.

Macfarlane, A. M. (1993), The chronology of tectonic events in the crystalline core of the Himalayas, Langtang National Park, central Nepal, *Tectonics*, *12*, 1004–1025.

Mancktelow, N. S., and B. Grasemann (1997), Time-dependent effects of heat advection and topography on cooling histories during erosion, *Tectonophysics*, *270*, 167–195.

Najman, Y., E. Garzanti, M. Pringle, M. Bickle, J. Stix, and I. Khan (2003), Early-middle Miocene paleodrainage and tectonics in the Pakistan Himalaya, *Geol. Soc. Am. Bull.*, *115*(10), 1265–1277.

Press, W. H., S. A. Teukolsky, W. T. Vetterling, and B. P. Flannery (1992), *Numerical Recipes in C: The Art of Scientific Computing*, 994 pp., Cambridge Univ. Press, New York.

Renne, P. R., C. C. Swisher, A. L. Deino, D. B. Karner, T. Owens, and D. J. DePaolo (1998), Intercalibration of standards, absolute ages and uncertainties in $^{40}Ar/^{39}Ar$ dating, *Chem. Geol.*, *145*, 117–152.

Searle, M. P., and L. Godin (2003), The south Tibetan detachment and the Manaslu leucogranite: A structural reinterpretation and restoration of the Annapurna-Manaslu Himalaya, Nepal, *J. Geol.*, *111*, 505–523.

Spiegel, C., J. Kuhlemann, I. Dunkl, W. Frisch, H. von Eynatten, and K. Balogh (2000), The erosion history of the central Alps: Evidence from zircon fis-

sion track data of the foreland basin sediments, *Terra Nova*, *12*, 163–170.

Stephens, M. A. (1965), The goodness-of-fit statistic V_n: Distribution and significance points, *Biometrika*, *52*, 309–321.

Stock, J. D., and D. R. Montgomery (1996), Estimating paleorelief from detrital mineral age ranges, *Basin Res.*, *8*, 317–327.

Strahler, A. N. (1952), Hypsometric (area-altitude) analysis of erosional topography, *Geol. Soc. Am. Bull.*, *63*, 1117–1141.

Stüwe, K., L. White, and R. Brown (1994), The influence of eroding topography on steady-state isotherms: Application to fission track analysis, *Earth Planet. Sci. Lett.*, *124*, 63–74.

Vermeesch, P. (2004), How many grains are needed for a provenance study?, *Earth Planet. Sci. Lett.*, *224*, 441–451.

Wagner, G. A., and G. M. Reimer (1972), Fission track tectonics: The tectonic interpretation of fission track apatite ages, *Earth Planet. Sci. Lett.*, *14*, 263–268.

Willett, S. D., and M. T. Brandon (2002), On steady states in mountain belts, *Geology*, *30*, 175–178.

K. V. Hodges and K. W. Ruhl, Department of Earth, Atmospheric and Planetary Sciences, Massachusetts Institute of Technology, 77 Massachusetts Ave, MIT Building 54-1022, Cambridge, MA 02139, USA. (kruhl@mit.edu)